Supporting Information

Hydrogen-Bonding Assisted Nano-Aggregation and Electropolymerization of C3-D-A-s-Triazine-2,4,6-triamide for High-Area-Capacitance Supercapacitors.

Chung-Yi Chang, [1] Man-kit Leung[*, 1, 2]

[*]Corresponding author. Tel.: +886 2 33661673; fax: +886 2 33668671.

[1] Department of Chemistry, National Taiwan University, Taipei 106319, Taiwan

[2] Institute of Polymer Science and Engineering, National Taiwan University, Taipei 106319, Taiwan

E-mail: mkleung@ntu.edu.tw (Prof. Man-kit Leung)

1. Experiment

The UV-Vis absorption spectra were measured in THF at room temperature. The concentration of **TRZ-A-TPA** was prepared and measured at 10^{-5} M. Cyclic voltammetry (CV) measurements of **TRZ-A-TPA** were carried out in dichloromethane at 10^{-3} M for oxidation, using an Ag/AgCl reference electrode. The reductive CV were carried out in dried DMF in the same concentration under deaerated conditions. The supporting electrolyte was tetrabutylammonium perchlorate (TBAP, 0.1 M). The scan rate was 100 mV s^{-1}. After each measurement, the CV redox potential of the Fc^{+}/Fc couple was used to recalibrate the electrical potential, thereby eliminating experimental errors. The CV spectra were realigned with respect to the Fc^{+}/Fc couple.

The E_{HOMO} levels are estimated according to electrochemical oxidation potential, using the Forrest approach. Assuming that the electrochemical behavior of our compounds follows the correlation equation of $E_{HOMO} = -(E_{OX}^{onset}-E_{Fc+/Fc})-4.8$ (eV) in CH_2Cl_2 versus an Ag/AgCl couple and $E_{Fc+/Fc} = 0.53$V. The E_{LUMO} (optical) has been estimated by the equation $E_{LUMO} = E_{HOMO} + E$(optical gap), and E(optical gap) was obtained by the equation: E(optical gap) = 1240.8/absorption λ_{onset} (nm).

2. Instrument

The UV-Vis was measured with a Hitachi U-3010 spectrophotometer. A nuclear magnetic resonance (NMR) spectrum was measured on a Varian Unity Plus (400 MHz). The chemical shifts in the proton nuclear magnetic resonance (1H NMR) and 13C nuclear magnetic resonance (13C NMR) spectra are reported in ppm on the δ scale, using CDCl3, acetone-d6, or DMSO-d6 as the solvent, as mentioned. In 1H NMR in $CDCl_3$ and $CHCl_3$, an impurity serves as the internal standard with a chemical shift of 7.23 ppm. When ^{13}C NMR was measured in $CDCl_3$, the chemical shift of $CDCl_3$, used as the internal standard, was 77 ppm. In 1H NMR measurements with DMSO-d6, $CD_2HS(O)CD_3$,

an impurity, serves as the internal standard with a chemical shift of 2.49 ppm. When ^{13}C NMR was measured in DMSO-d_6, the chemical shift's internal standard is 39.7 ppm. The definitions of splitting are listed: singlet (s); doublet (d), triplet (t), quartet (q), broad (br), and multiplet (m). The coupling constant is expressed in J in Hz. Infrared spectroscopy was measured by Jasco FT/IR-480. The liquid sample was measured by coating on KBr under neat conditions. The solid sample was measured in a KBr pellet. The unit is wavenumber cm^{-1}. Bruker, New UltrafleXtremeTM, Bremen, D.E., measured MALDI-TOF mass spectrometry. TGA was measured with a TA2950 Thermogravimetric Analyzer. Cyclic voltammetry was measured using the Squidstat Plus station. SEM (scanning electron microscope) images were analyzed using a Hitachi SU8000.

Specific capacitance measurement

Specific capacitance of **pTRZ-A-TPA** was measured in three electrolyte systems with ITO (10 Ω) as the working electrode. The polymer films were prepared by cyclic voltammetry for 100 cycles, which is the same as in the glassy carbon system. The specific capacitance was measured by converting the area current to weight current using an area mass of 0.62 mg cm^{-2}.

Experiment of pTRZ-AA-TPA film area mass

The **pTRZ-A-TPA** films used for the mass measurement test were prepared by cyclic voltammetry over 100 cycles. The active area of the **pTRZ-A-TPA** film used for mass measurement was about 2.1 cm^2. Mettler Toledo AG245 Analytical Balance tested the mass of **pTRZ-A-TPA** film, and the average value of mass was about 0.61±0.02 mg, while the area mass is 0.29±0.01 mg cm^{-2}

3. Synthetic Procedures

The detailed synthetic routes for **pTRZ-A-TPA** are summarized in **Figure S1**. **TPA-NH_2** (**2**) was prepared according to literature procedures [1, 2], and **H3TATB** (**4**) was synthesized through acid-

catalyzed cyclization of p-tolunitrile, followed by Stork's oxidation [3]. **H3TATB** was then converted to the corresponding acyl chloride **TATBCl** (**5**) and coupled with **TPA-NH_2** (**2**) to give **TRZ-A-TPA**. The polymer **pTRZ-A-TPA** was prepared from **TRZ-A-TPA** via oxidative polymerization or electrochemical deposition methods.[4] The procedures are attached on pp. S5-S10. The ^{1}H NMR of **2-4**, and ^{1}H and ^{13}C NMR of **H3TATB**, and MALDI-TOF mass spectrum of **TRZ-A-TPA** are attached in **Figures S2-S6**.

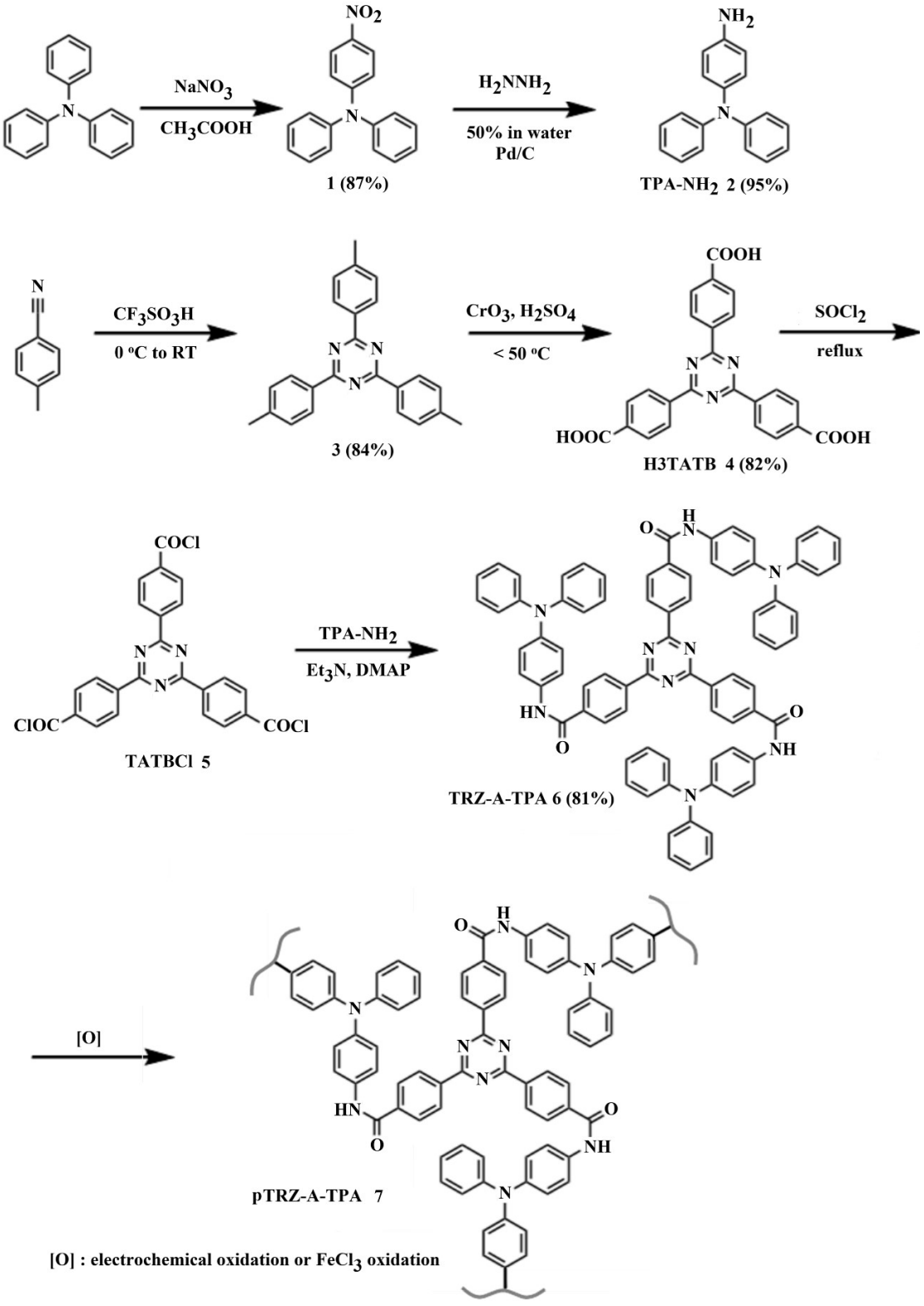

Figure S1. Comprehensive synthetic scheme of the **TRZ-A-TPA** monomer and the **pTRZ-A-TPA** polymer. The route illustrates the synthesis of key intermediates (**TPA-NH₂** and **H3TATB**), their coupling to form the monomer (6), and the subsequent oxidative polymerization to construct the crosslinked network (7).

4-Nitrotriphenylamine (1)

To a two-necked flask equipped with a reflux condenser was charged triphenylamine (500 mg, 2.04 mmol) in a mixture of glacial acetic acid (18 mL) and chloroform (6 mL). $NaNO_3$ (171.6 mg, 2.02 mmol) was then added. The reaction mixture was stirred and heated at 90° C for 2 h. After that, the mixture was cooled to rt. The mixture was diluted with water (50 mL) and extracted with dichloromethane (50 mL) several times. The organic extracts were combined and washed with brine (25 mL) three times, treated with anhydrous $MgSO_4$, filtered, and concentrated under reduced pressure to give a crude oil, which was crystallized from ethanol:H_2O (25 mL, 1:1) to afford **1** as an orange crystalline solid (515.3 mg, 1.54 mmol, 87%). The ^{1}H NMR data are consistent with those reported in the references [1].

4-Aminotriphenylamine (**2**)

To the reflux apparatus was charged Pd/C (5.0 mg) in anhydrous ethanol (5.0 mL) followed by **1** (500 mg, 1.72 mmol). The mixture was stirred and heated at reflux. Hydrazine monohydrate (0.50 mL**,** 32 mmol) was added dropwise to the hot solution. The reaction was refluxed for an additional 2 h. The hot reaction mixture was filtered over a celite pad and washed with dichloromethane several times. The filtrate was dried over anhydrous $MgSO_4$, filtered, and concentrated under reduced pressure to give a crude solid, which was further recrystallized from ethanol:H_2O (3:1) to yield a grayish solid (426 mg, 1.64 mmol, 95%). ^{1}H NMR (400 MHz, d6-DMSO): δ 7.19 (t, J = 8 Hz, 4H), 6.88 (m, 6H), 6.79 (d, J = 8 Hz, 2H), 6.55 (d, J = 8 Hz, 2H), 5.07(s, 2H).[1]

2,4,6-Tris(4′,4",4"′-trimethylphenyl)-1,3,5-triazine (**3**)

A mixture of *para*-tolunitrile (10.00 g, 0.85 mol) and trifluoromethane sulfonic acid (34.0 g, 0.23

mol) was stirred at 0 °C for 30 min. The mixture was further stirred at room temperature overnight. Ice-water (20 ml) was added to quench the reaction. The mixture was then neutralized with NaOH (10 mL) to give a white precipitate. Compound **3** was obtained after filtration and recrystallization from chloroform to give white needle-shaped crystals (8.43 g, 0.239 mol, 84.3%).^{1}H and ^{13}C NMR data are consistent with those reported in the reference.[3]

2,4,6-Tris-(*para*-carboxyphenyl)-1,3,5-triazine (H3TATB)

To a two-necked flask (500 mL) was charged a mixture of acetic acid (72.64 g, 1.20 mmol) and concentrated sulfuric acid (4.4 mL). Compound **3** (2.78 g, 7.9 mmol) was added, followed by chromium (VI) oxide (7.2 g, 72 mmol) and acetic anhydride (5.18 g, 51 mmol), both added slowly. The mixture was stirred and kept below 50 °C. Note that chromium(VI) oxide is potentially carcinogenic and must be used with caution. The resulting dark brown slurry was stirred overnight and subsequently quenched by pouring into 300 mL of ice-cold water. After thorough mixing, the precipitate was collected via filtration, washed repeatedly with distilled water, and finally re-dissolved in a 2 M NaOH aqueous solution (200 mL). The undissolved materials were removed by filtration. The filtrate was acidified with hydrochloric acid to give a crude product. Recrystallization of the crude material from DMF yielded the desired product, **H3TATB**, as a white solid (yield: 82%). ^{1}H NMR (400 MHz, d_6-DMSO): δ 8.82 (d, J = 8.0 Hz, 6H), 8.18 (d, J = 8 Hz, 6H).[3]

TATBCl (5)

TATBCl was prepared by refluxing **H3TATB** (1.00, 2.2 mmol) in a thionyl chloride solution (5 mL) with stirring. Note that thionyl chloride is poisonous and must be used carefully. Six drops of dry

DMF were added as a catalyst. The reaction was carried out overnight under N_2 atmosphere. The excess thionyl chloride was removed by vacuum distillation. **TATBCl** was collected and used directly for the next step without purification.

TRZ-A-TPA (6)

TATBCl (1.0 mmol) in dried dichloromethane (5 mL), *N,N*-dimethylaminopyridine (DMAP) (6.23 mg, 0.051 mmol) in dried dichloromethane (5 mL), triethylamine (1.1 mL), and **2** (0.90g, 3.45 mmol) were mixed under argon. The mixture was refluxed for 24 h. The mixture was quenched by adding water. The product was extracted with DCM several times. The organic extracts were dried over $MgSO_4$. After removal of the solvent under vacuum, the crude product was purified by recrystallization from DCM/MeOH to give **TRZ-A-TPA** (81%). ^{1}H-NMR (400 MHz, d_6-DMSO): δ 10.49 (s, 3H), 8.88 (d, J=8 Hz, 6H), 8.21 (d, J=12 Hz, 6H), 7.77 (d, J=8 Hz, 6H), 7.29 (t, J=6 Hz, 12H), 7.06-6.98 (m, 24H); ^{13}C-NMR (400 MHz, d6-DMSO): δ 171.19, 165.15, 147.85, 143.54, 139.42, 138.24, 135.08, 129.96, 129.32, 128.79, 125.33, 123.64, 123.02, 122.38 (14 sets of aromatic carbon NMR signal were recorded). MALDI-TOF m/z calcd for M $C_{78}H_{57}N_9O_3$ 1167.4584 found 1167.4610

pTRZ-A-TPA (7) by oxidation polymerization

$FeCl_3$ (34.0 mg, 0.214 mmol) and chloroform (0.17 ml) were added to **TRZ-A-TPA (6)** (100 mg, 0.086 mmol). The solution was stirred at 55˚C in an inert atmosphere for 22 h and quenched by pouring into a mixture (4:1) of methanol and hydrochloric acid (1 M). The precipitate was collected and washed thoroughly with aqueous NH_4OH, and then with methanol and deionized water 3 times to afford **pTRZ-A-TPA.**

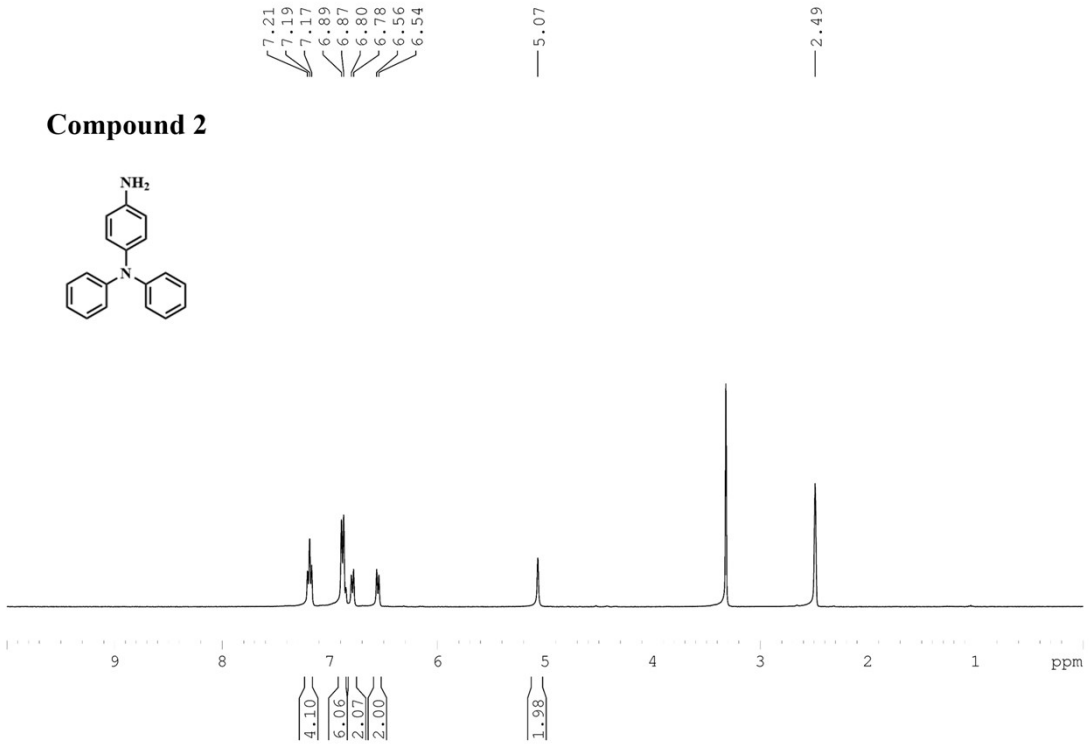

Figure S2. ^{1}H NMR analysis of TPA-NH_2

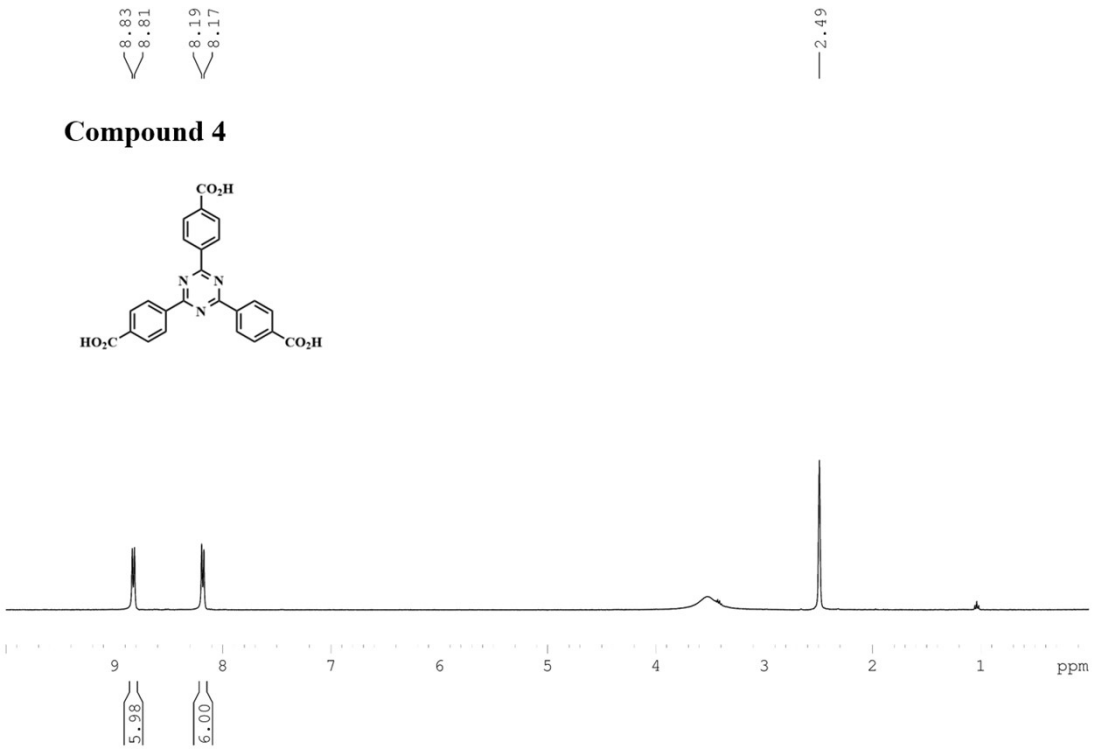

Figure S3. ^{1}H NMR analysis of H3TATB

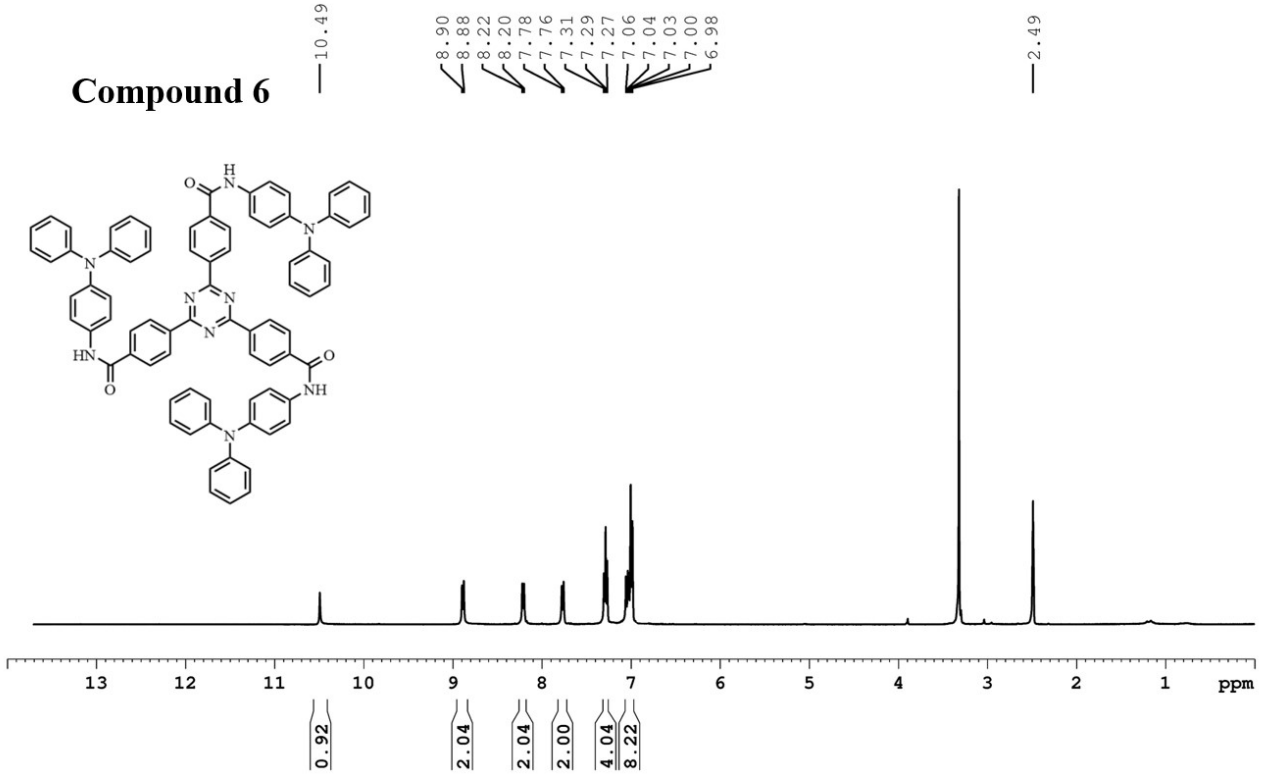

Figure S4. ^{1}H NMR analysis of TRZ-A-TPA

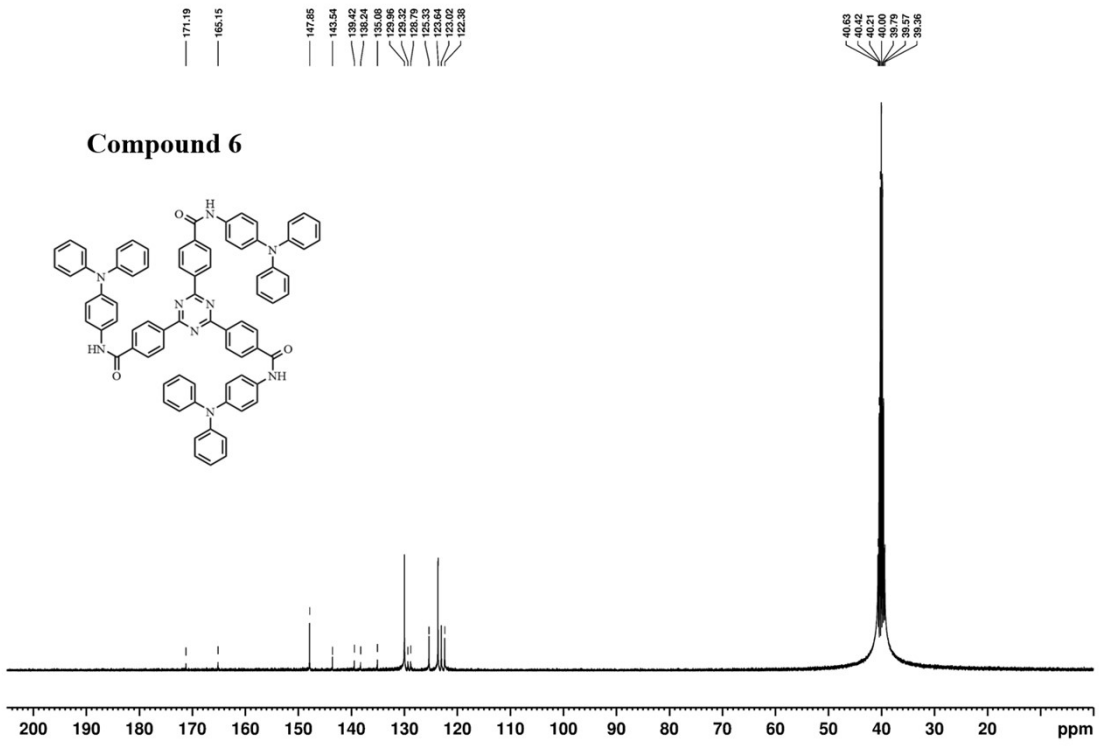

Figure S5. ^{13}C NMR analysis of TRZ-A-TPA

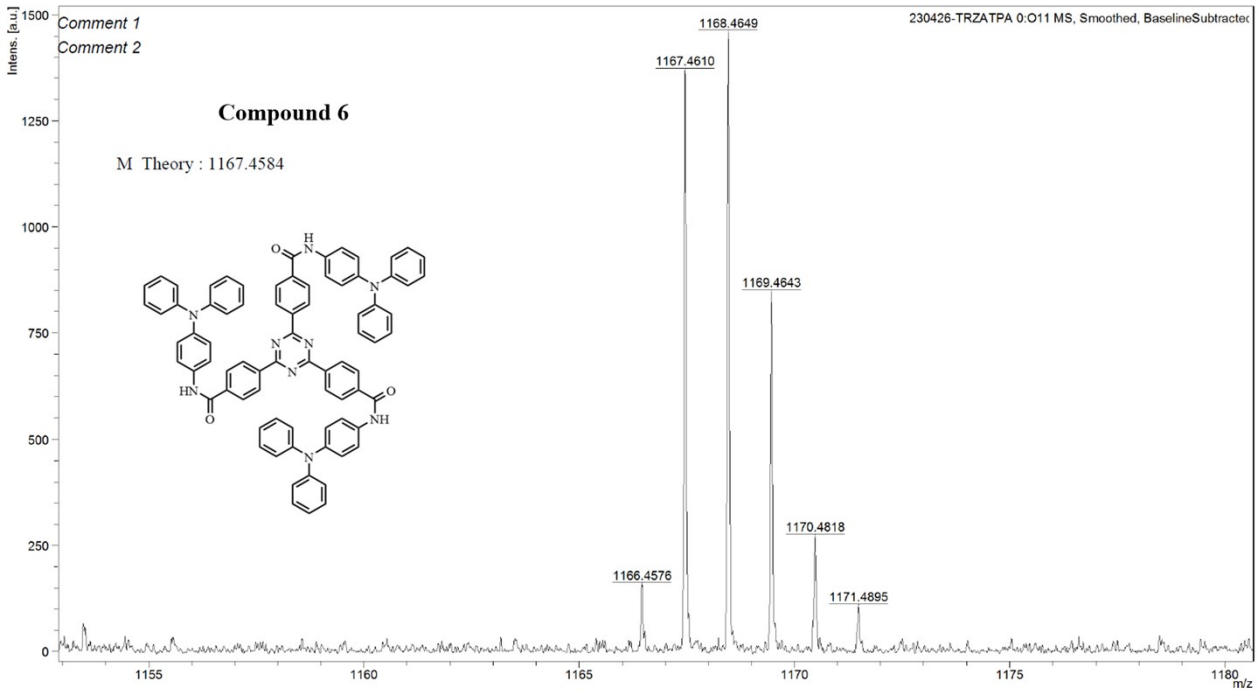

Figure S6 MALDI-TOF spectrum of TRZ-A-TPA

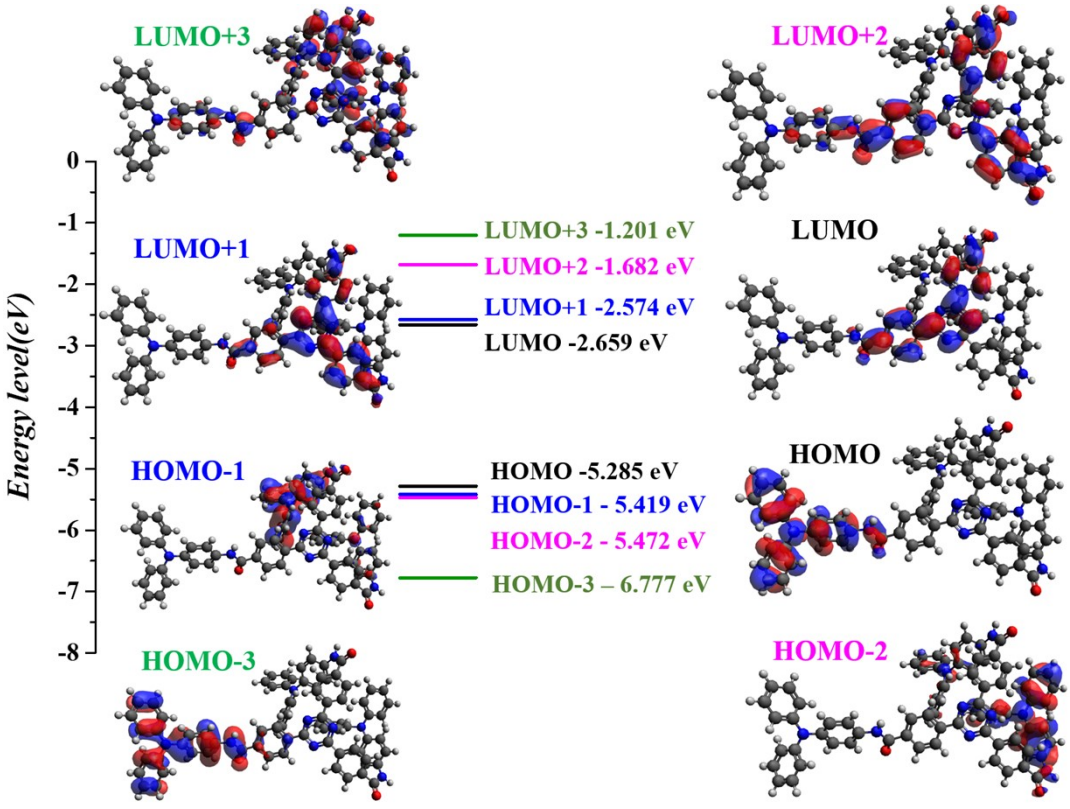

Figure S7. Calculated energy level diagram and spatial electron density distributions of the frontier molecular orbitals (ranging from HOMO-3 to LUMO+3) for the **TRZ-A-TPA** monomer. The results

were obtained from Density Functional Theory (DFT) calculations utilizing the B3LYP-D3 functional basis set.

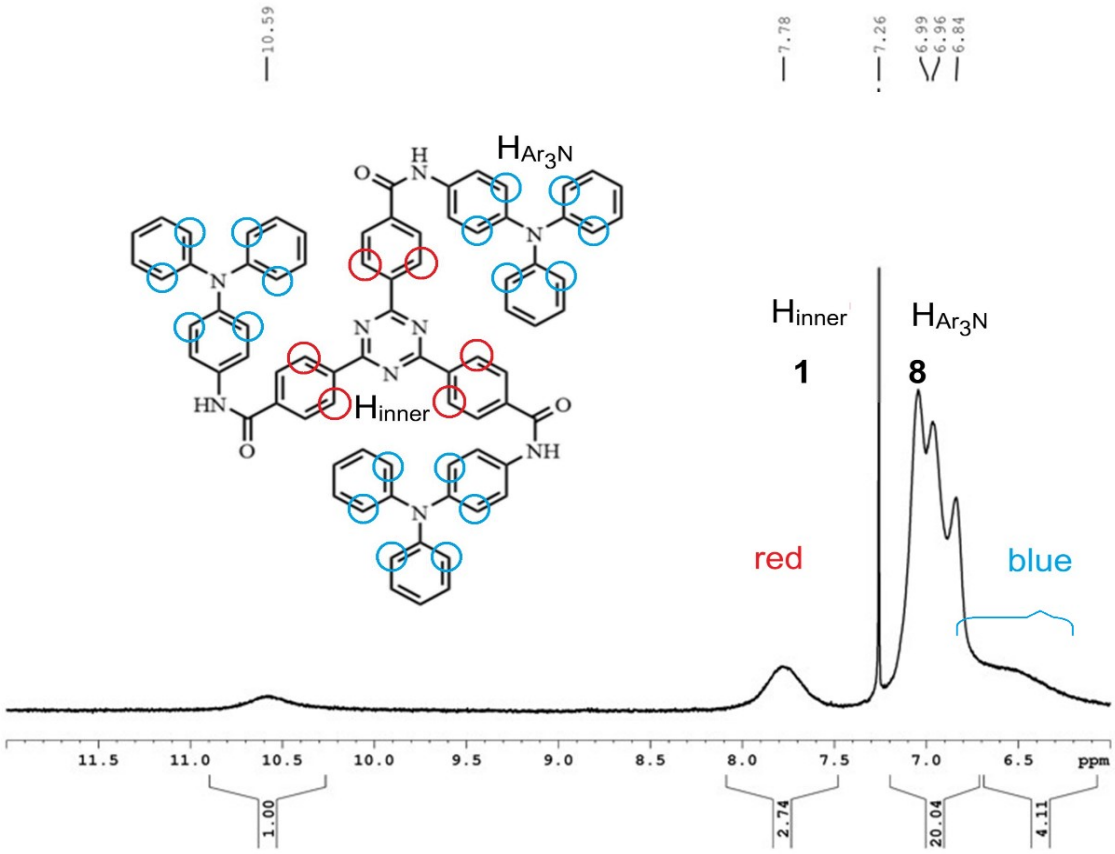

Figure S8. ^{1}H NMR of **TRZ-A-TPA** in $CDCl_3$

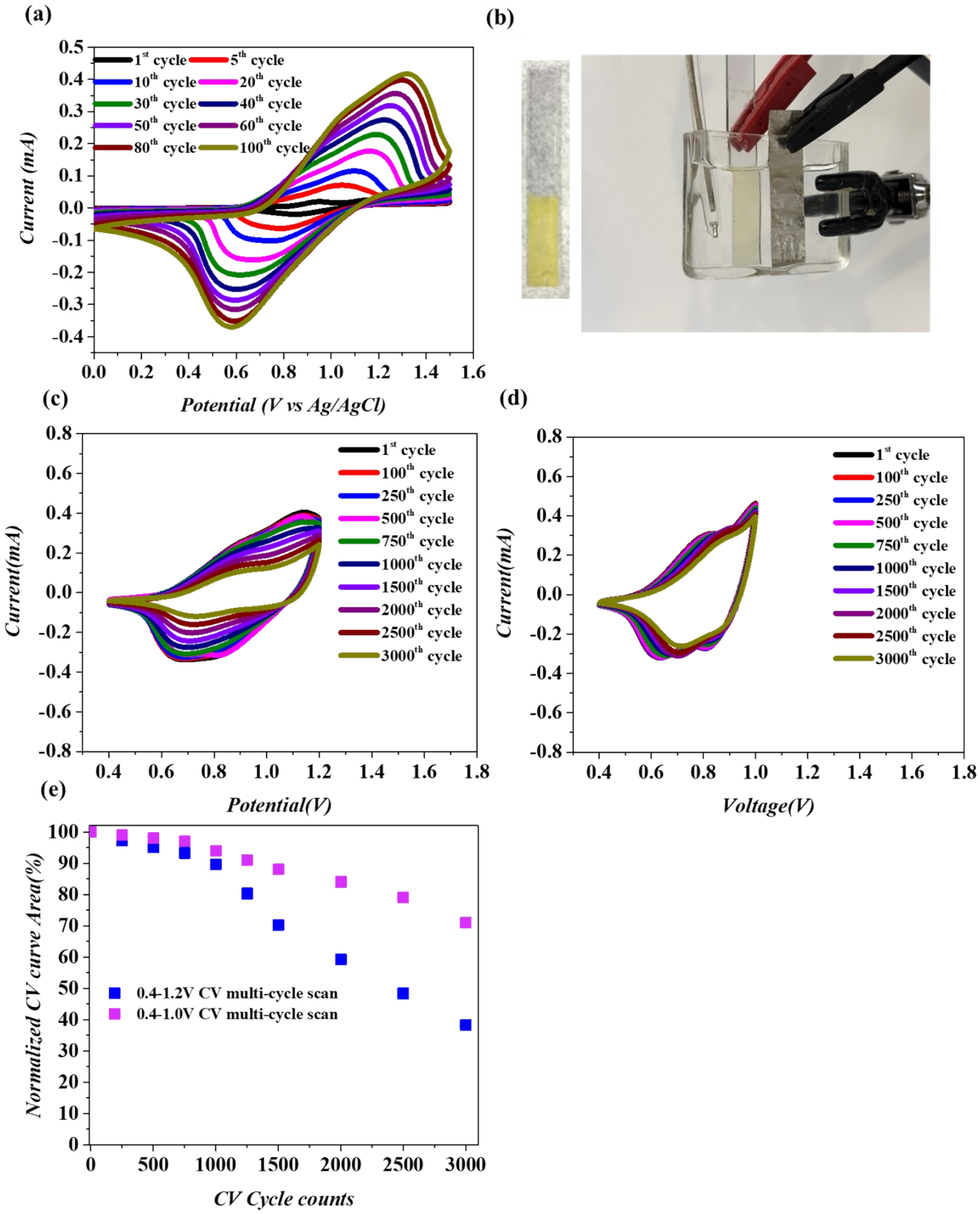

Figure S9. Electrochemical synthesis and voltage-dependent long-term cycling stability of the **pTRZ-A-TPA** film. (a) Continuous cyclic voltammograms (100 cycles) during the in-situ electropolymerization of the **TRZ-A-TPA** monomer on an ITO working electrode. (b) Optical photographs of the resulting uniform **pTRZ-A-TPA** film deposited on the ITO substrate at 20 cycle sweep CV scan. Evolution of the CV curves over 3,000 continuous cycles tested in a monomer-free 0.1 M $TBAPF_6$/DCM electrolyte under different potential windows: (c) 0.4 to 1.2 V and (d) 0.4 to 1.0

V. (e) Comparison of the capacitance retention (normalized CV curve area) over 3,000 cycles, explicitly demonstrating that restricting the upper anodic potential limit to 1.0 V significantly mitigates structural degradation and enhances the operational stability compared to the 1.2 V window**.**

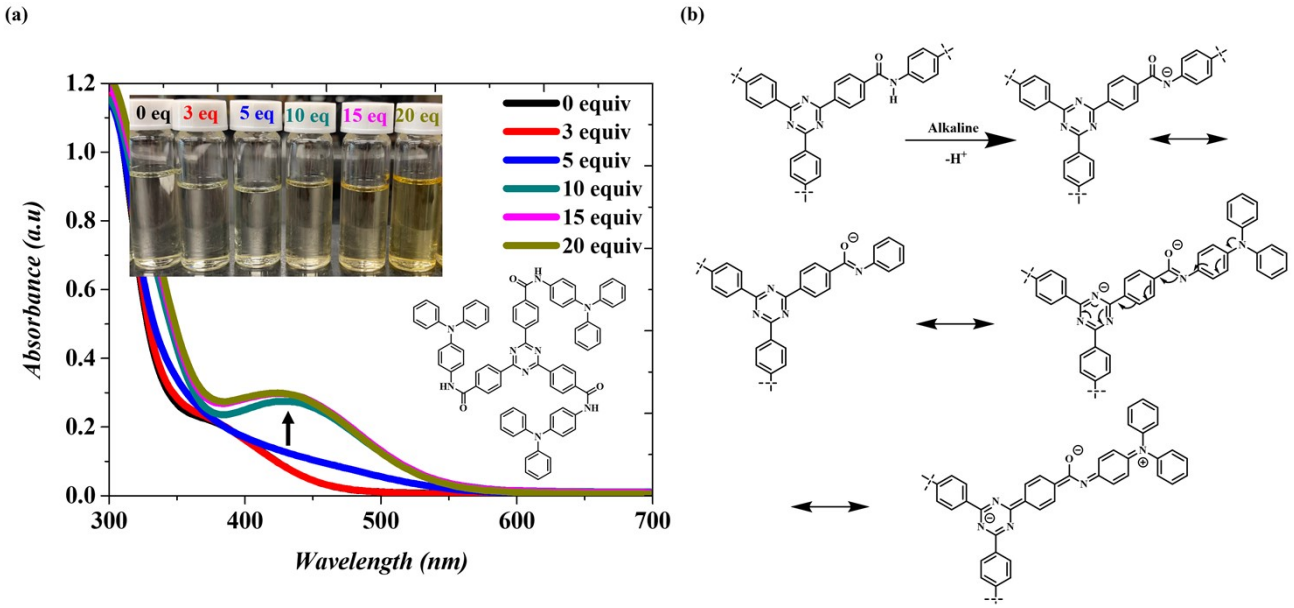

Figure S10. Alkaline-induced deprotonation effect on **TRZ-A-TPA**. (a) UV-vis titration spectra of **TRZ-A-TPA** upon adding varying equivalents of TMAH in THF, showing a new absorption band and macroscopic color change (inset). (b) Proposed mechanism depicting the deprotonation of the amide N-H bond and the subsequent resonance stabilization of the anion, which rationalizes the observed optical changes and the disruption of hydrogen-bonded nano-aggregates.

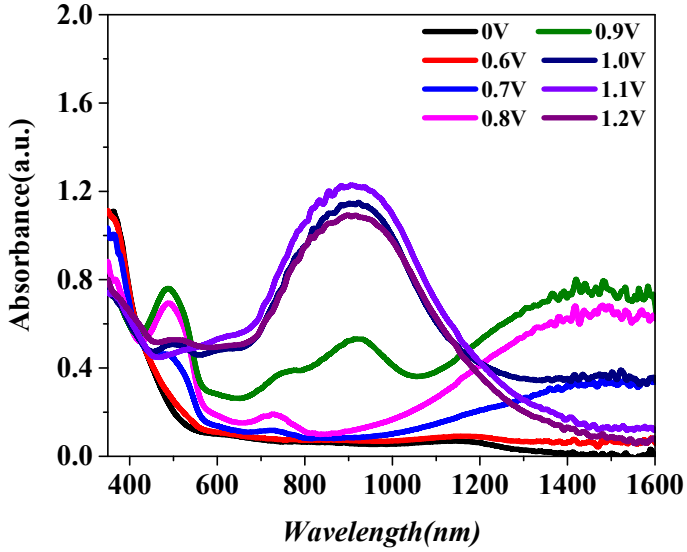

Figure S11. In-situ UV-Vis-NIR spectra of the **pTRZ-A-TPA** film tested in a 0.1mM $TBAPF_6$

solution under applied potentials from 0 to 1.2 V. The emergence of absorption bands at ~490 nm and > 1300 nm (at 0.8–0.9 V) indicates the formation of the TPB radical cation. The subsequent dominant peak at ~900 nm (at > 1.0 V) corresponds to the TPB dication. These characteristic spectral shifts directly confirm the para-to-para benzidine coupling pathway.

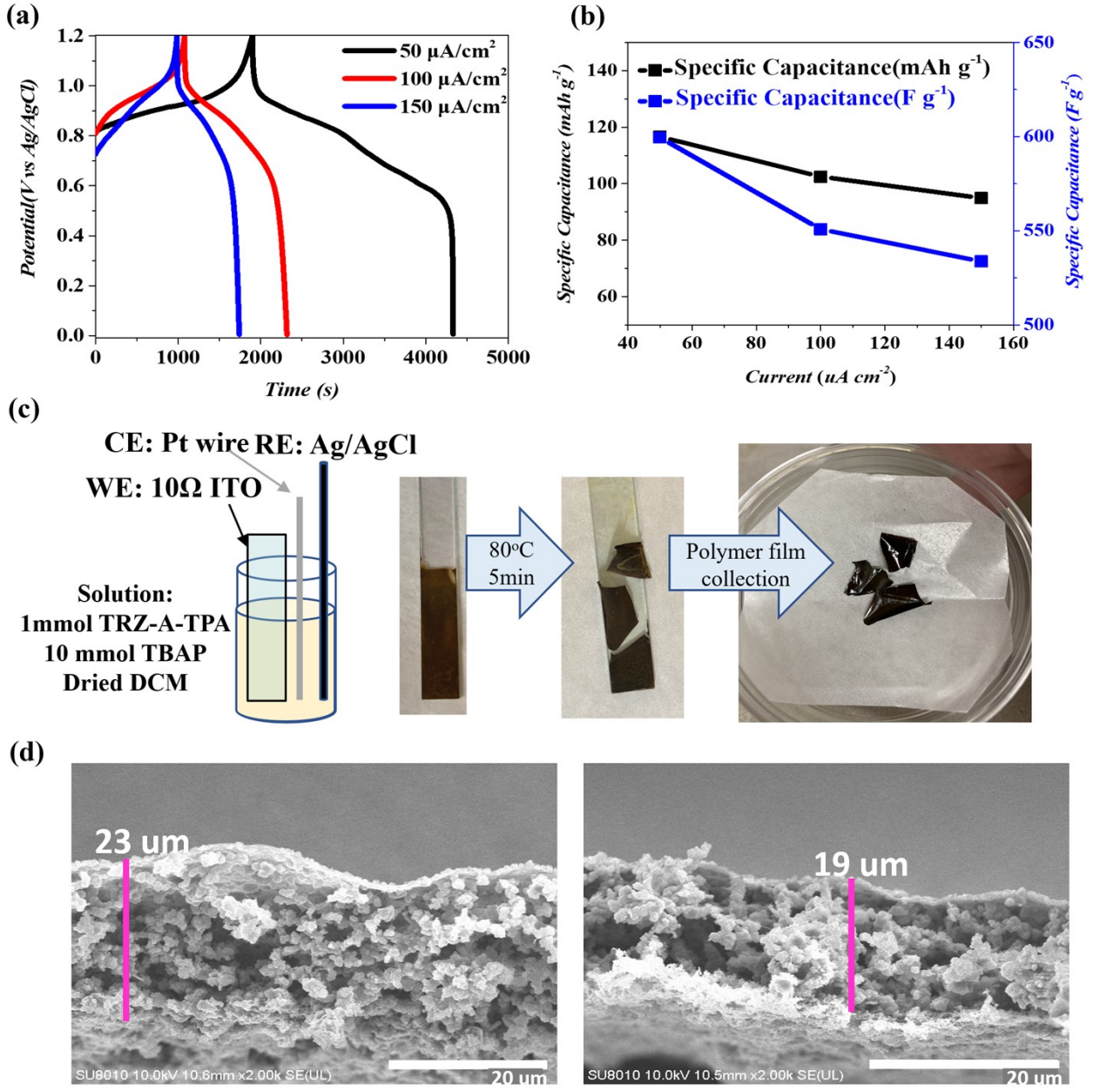

Figure S12. (a) GCD profiles of the **pTRZ-A-TPA** film at various current densities in $TABPF_6$/DCM. (b) Calculated gravimetric specific capacitance plotted against current density, expressed in both mAh g^{-1} and F g^{-1}. (c) Schematic setup for electropolymerization and photographic demonstration of the thermal peeling process (80 °C) to obtain a free-standing **pTRZ-A-TPA** polymer film from the ITO working electrode. (d) Cross-sectional SEM image of the free-standing **pTRZ-A-TPA** film after 100 CV cycles, revealing a substantial macro-scale thickness of ~20 μm while maintaining an interconnected porous architecture.

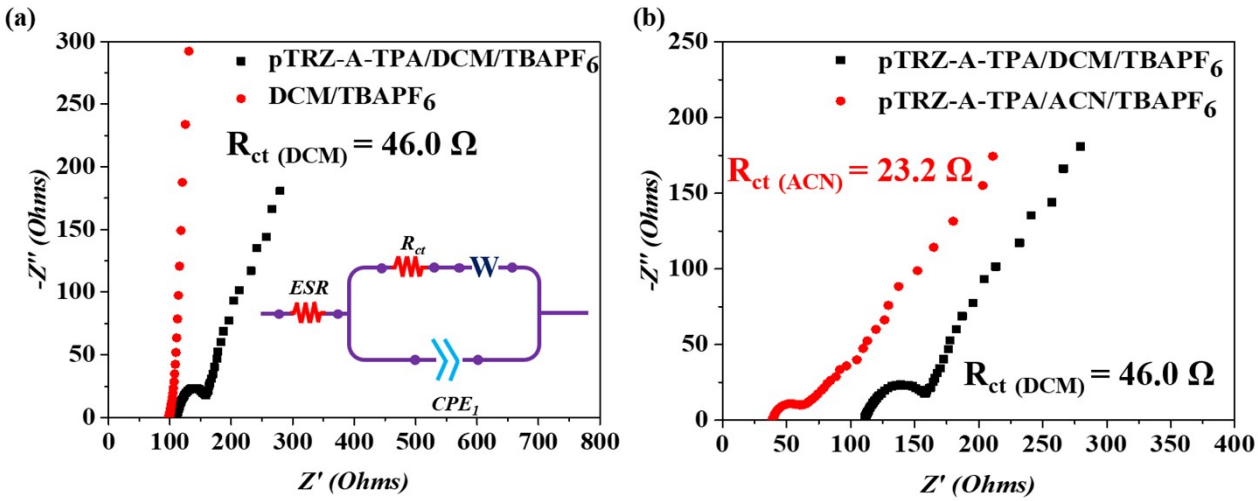

Figure S13. impedance results (Nyquist plot) of the **pTRZ-A-TPA** film (the inset shows the Randles equivalent circuit fit to the experimental EIS data); (a)**pTRZ-A-TPA** in DCM/$TBAPF_6$ and ACN/$TBAPF_6$ (b) **pTRZ-A-TPA** in DCM/$TBAPF_6$ and ACN/$TBAPF_6$

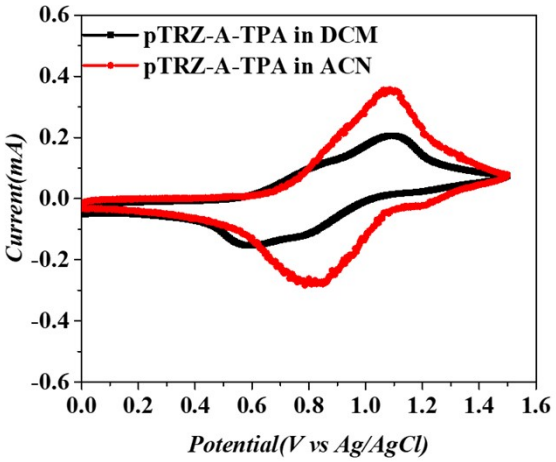

Figure S14. Cyclic voltammetry data of **pTRZ-A-TPA** film in DCM/$TBAPF_6$ and ACN/$TBAPF_6$

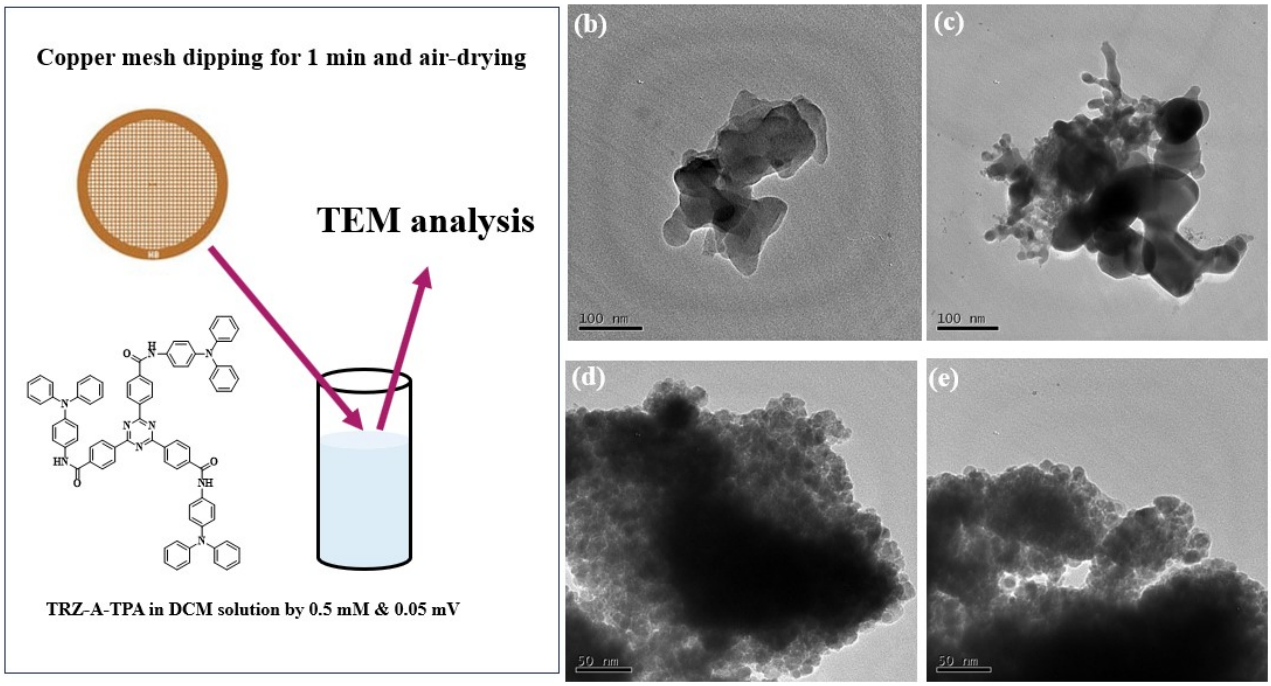

Figure S15. (a)TEM Sample preparation procedure (b)(c)TEM results of **TRZ-A-TPA** at 0.5 mM in DCM (d)(e)TEM results of **TRZ-A-TPA** at 0.05 mM in DCM

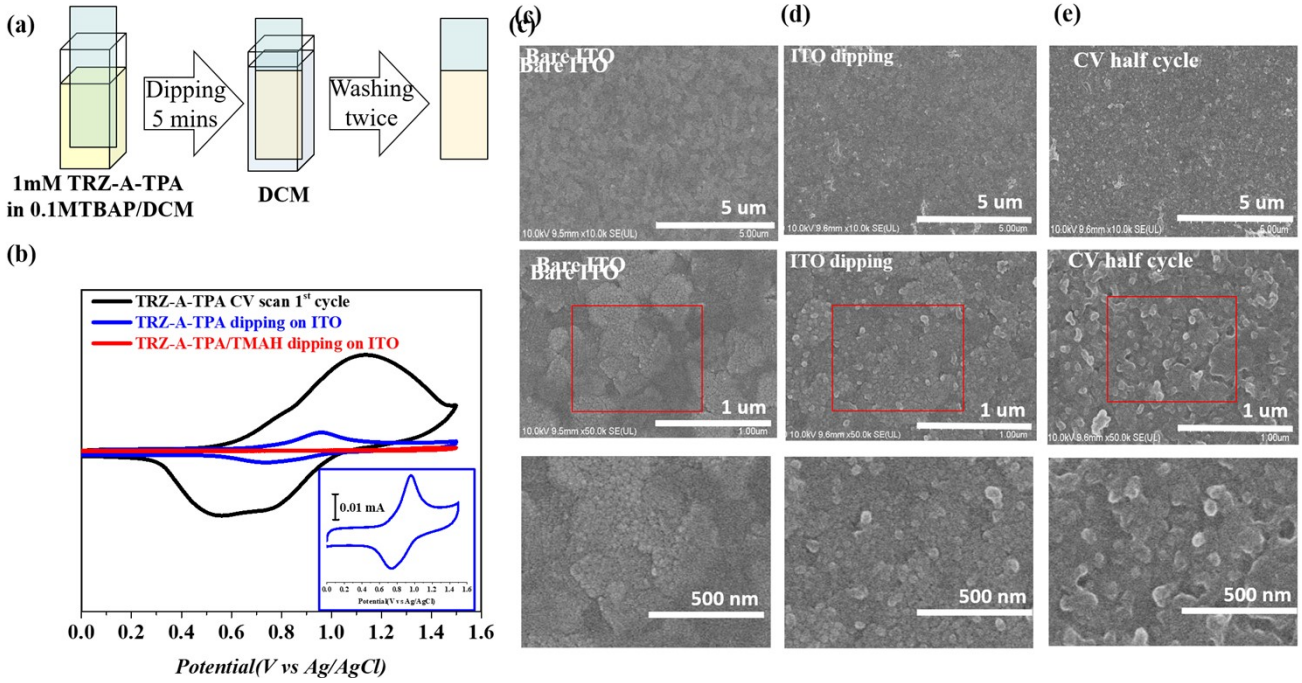

Figure S16. Interfacial adsorption and morphological evolution of **TRZ-A-TPA**. (a) Schematic of the dipping and washing process on an ITO electrode. (b) CV curves of the half CV cycle (black) measured in a 0.1 M $TBAPF_6$/DCM solution, and the dip-coated ITO tested in a 0.1 M $TBAPF_6$/DCM e solution (blue, the inset shows magnified peaks). SEM images of (c) bare ITO, (d) dip-coated ITO showing adsorbed nano-aggregates, and (e) the electrode surface after a half CV cycle, observed at three different magnifications.

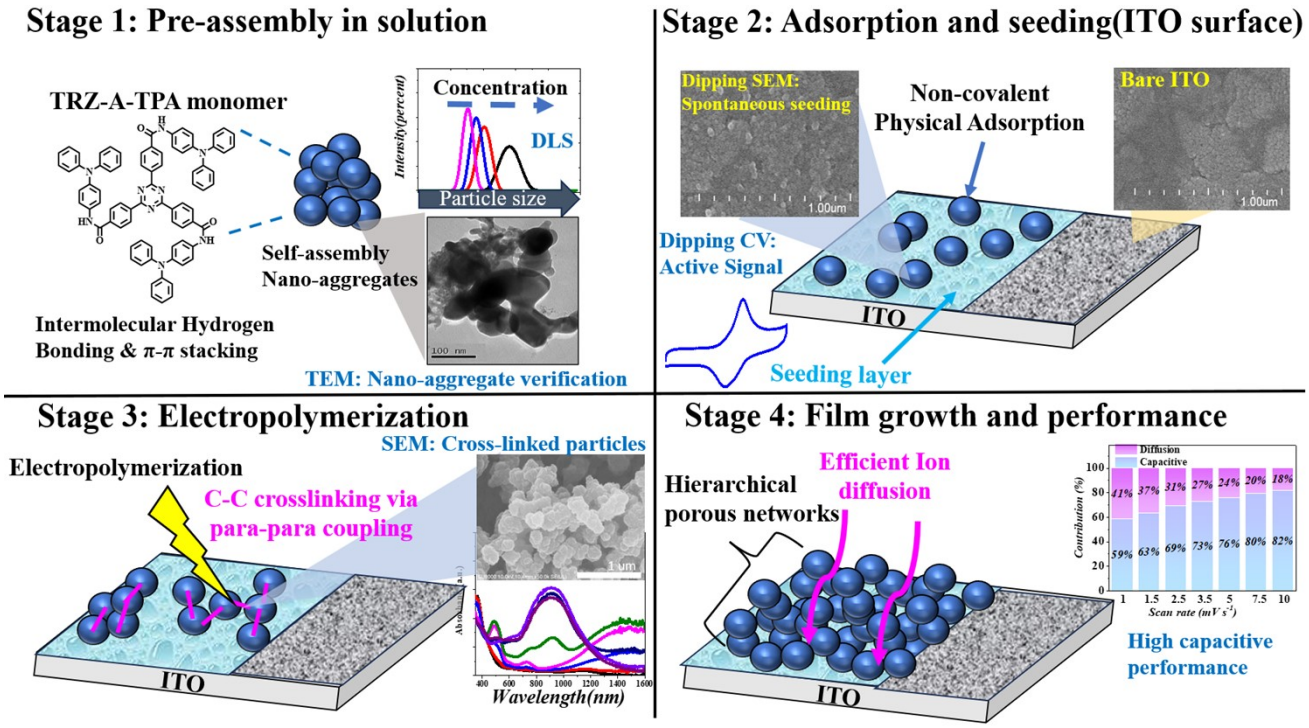

Figure S17. Mechanistic summary of the additive-free electrode fabrication. **Stage 1:** Pre-assembly of **TRZ-A-TPA** monomers into nano-aggregates driven by hydrogen bonding and π-π stacking. **Stage 2**: Spontaneous physical adsorption and seeding of aggregates onto the ITO surface. **Stage 3**: In-situ electropolymerization welding the pre-adsorbed seeds via para-para benzidine coupling. **Stage 4**: Formation of a hierarchically porous network enabling fast ion diffusion and high pseudocapacitive performance.

Table S1. Electrochemical performance comparison of TPA-based materials in organic electrolytes

TPA based polymer	Working Electrode	Electrolyte	Specific Capacitance (Current Density)	Cycling stability (Cycles/Retention%)	Reference
P1	ITO	$LiClO_4$/PC	21.59 mF cm^{-2}(0.075 mA cm^{-2})	100 cycles 60.0%	[5]
pTTPACB	ITO	$TBAPF_6$/DCM	6.64 mF cm^{-2}(0.05 mA cm^{-2})	1000/2000 cycles 84%/77%	[6]
PTPAP-BY	ITO	$TPAPF_6$/Tol:ACN	7 mF cm^{-2}(0.06 mA cm^{-2})	60 cycle 70%	[7]
PETOME	ITO	$LiClO_4$ ACN	36.2 mF cm^{-2}(0.10 mA cm^{-2})	5000 cycles 80.6%	[8]
TPPA-Me-TB	ITO	TBABF4/MeCN	165.3 F g^{-1}(1A g^{-1})	500 cycles 86.6%	[9]
p-HPB-6TPA	Glassy carbon	$LiClO_4$ ACN	170 mF cm^{-2}or 788.9 F g^{-1} (0.10 mA cm^{-2})	1000/1500 cycles 90%/85%	[10]
LPA	ITO	$TBABF_4$/MeCN	7.52 mF cm^{-2} or 117.5 Fg^{-1} (1.0 A g^{-1})	20 cycles 20%	[11]
pPh-4TPA	ITO	$TBAPF_6$/ACN	423 F g^{-1} (20 A g^{-1})	500 cycles 65.4 %	[12]
PHHTPA	ITO	$TBABF_4$/MeCN	3.17 mF cm^{-2}(0.08 mA cm^{-2})	200 cycles 90%	[13]
pTRZ-A-TPA	Glassy carbon or ITO	$TBAPF_6$/DCM TBAPF6/ACN	218 mF cm^{-2} or 599.5 F g^{-1} (0.05 mA cm^{-2})	1.2V 1000/3000 cycles 87%/40% 1.0V 1000/3000 cycles 94%/70%	this work

Table S2. Electrochemical performance comparison of TPA-based materials in aqueous electrolytes

TPA based polymer	Working Electrode	Electrolyte	Specific Capacitance (Current Density)	Cycling stability (Cycles/Retention%)	Reference
TPA-TBP-CMP	Glassy carbon	KOH solution	356 F g^{-1} (1 A g^{-1})	1000/2000 cycles 97%/90%	[14]
TPA-IM-AQ	Graphite foil	H_2SO_4 solution	275.72 F g^{-1}(0.5 A g^{-1})	5000 cycles 88.4%	[15]

References

[1] M.I. Mangione, R.A. Spanevello, M.B. Anzardi, Efficient and straightforward click synthesis of structurally related dendritic triazoles. RSC Adv., 7 (2017) 47681–47688.

[2] E. Moulin, F. Niess, M. Maaloum, E. Buhler, I. Nyrkova, N. Giuseppone, The Hierarchical Self-Assembly of Charge Nanocarriers: A Highly Cooperative Process Promoted by Visible Light. Angew. Chem. Int. Ed., 49 (2010) 6974–6978.

[3] M. Krüger, H. Reinsch, A.K. Inge, N. Stock, Effect of partial linker fluorination and linker extension on structure and properties of the Al-MOF CAU-10. MICROPOR MESOPOR MAT, 249 (2017) 128–136.

[4] Y.N. Luponosov, A.N. Solodukhin, I.A. Chuyko, S.M. Peregudova, S.A. Ponomarenko, Highly electrochemically and thermally stable donor–π–acceptor triphenylamine-based hole-transporting homopolymers via oxidative polymerization. New J. Chem., 46 (2022) 12311–12317.

[5] P. Wang, Y. Sun, J. Li, G. Zhu, X. Zhang, H. Yang, B. Lin, Electrode materials for flexible supercapacitor with real-time visual monitoring of potential. Chem. Eng. J., 446 (2022) 137330.

[6] M. Shao, X. Lv, C. Zhou, M. Ouyang, X. Zhu, H. Xu, Z. Feng, D.S. Wright, C. Zhang, A colorless to multicolored triphenylamine-based polymer for the visualization of high-performance electrochromic supercapacitor. Sol. Energy Mater. Sol. Cells., 251 (2023) 112134.

[7] Y. Pan, P. Gao, H. Chen, X.-P. Zhang, Y. Han, Z. Gu, J. Xu, R. Zhang, J. Liu, Electropolymerization of D-A type monomers consisting of mono-triphenylamine moiety for electrochromic devices and supercapacitors. J. Mol. Struct., 1292 (2023) 136182.

[8] Y. Xie, Y. Zhang, M. Zhu, R. Huang, D. Chao, High-performance electrochromic supercapacitor based on a new EDOT-triphenylamine conjugated polymer. Dyes Pigm., 208 (2023) 110889.

[9] Y.-J. Shao, T.-C. Yen, C.-C. Hu, G.-S. Liou, Non-conjugated triarylamine-based intrinsic microporous polyamides for an electrochromic supercapacitor: diffusion dynamics and charge–discharge studies. J. Mater. Chem. A, 11 (2023) 1877–1885.

[10] B. Wang, L. Wang, H. Chen, Y. Jia, Y. Ma, Electropolymerized Triphenylamine Network Films for High-Performance Transparent to Black Electrochromism and Capacitance. Adv. Opt. Mater., 11 (2023) 2201572.

[11] Y.-J. Shao, Y.-J. Cho, H.-L. Li, C.-C. Hu, G.-S. Liou, Non-conjugated electrochromic supercapacitors with atom-economic arylamine-based AB2-polyamides. J. Mater. Chem. A, 12 (2024) 20327–20336.

[12] Q. Huang, J. Chen, X. Shao, L. Zhang, Y. Dong, W. Li, C. Zhang, Y. Ma, New

electropolymerized triphenylamine polymer films and excellent multifunctional electrochromic energy storage system materials with real-time monitoring of energy storage status. Chem. Eng. J., 461 (2023) 141974.
[13] Z. Duan, Q. Guo, J. Cui, C. Ma, Y. Han, J. Liu, Electrochemical polymerization of V-shape triphenylamine-based monomers for multicolor electrochromism and energy storage devices. Polymer, 338 (2025) 129047.
[14] M.G. Kotp, J. Lüder, S.-W. Kuo, A.F.M. El-Mahdy, Phenazine-integrated conjugated microporous polymers for modulating the mechanics of supercapacitor electrodes. Mater. Adv., 5 (2024) 4142–4150.
[15] S.D. Jagadale, S.V. Bhosale, Organic Electrode Material Based on Tris-Imidazole Ring Containing Triphenylamine (Donor)-Anthraquinone (Acceptor) for High Performance Pseudocapacitors. Chem. Eur. J., 31 (2025) e202500723.